Continuous-time, high-cycle fatigue model: Validity range and computational acceleration for cyclic stress

Stefan Lindström, Carl-Johan Thore, Shyam Suresh and Anders Klarbring

Lindström, S., Thore, C., Suresh, S., Klarbring, A., (2020), Continuous-time, high-cycle fatigue model: Validity range and computational acceleration for cyclic stress, *International Journal of Fatigue*, 136, 105582. https://doi.org/10.1016/j.ijfatigue.2020.105582

Continuous-time, high-cycle fatigue model: Validity range and computational acceleration for cyclic stress

Stefan B. Lindström[a,*], Carl-Johan Thore[a], Shyam Suresh[a], Anders Klarbring[a]

[a]*Division of Solid Mechanics, Department of Management and Engineering, Institute of Technology, Linköping University, 581 83 Linköping, Sweden*

Abstract

The properties of the continuous-time, high-cycle fatigue model of Ottosen *et al.* [Int. J. Fatigue, 30:996–1006 (2008)] is investigated for challenging stress states. We derive an analytical solution to the damage per cycle for cyclic, proportional stress. Numerical investigations for 7050-T7451 aluminum alloy and AISI 4340 steel alloy show exponential convergence to a constant damage per cycle for cyclic proportional stress, and Wynn's epsilon algorithm for sequence acceleration improves the convergence rate. Fatigue damage is well predicted for an applied proportional stress, but damage is severely underpredicted for rotary stress states or combinations of tension/compression and torsion.

Keywords: High-cycle fatigue, Nonproportional stress, Fatigue model

1. Introduction

Fatigue in metals is a complicated system phenomenon that depends on many factors including surface treatment and surface roughness, environmental conditions, component size and related stress gradient effects. Even with all these factors taken to be constant, predicting the fatigue life resulting from a general stress history is a challenging problem. Most fatigue models are based on cycle-counting algorithms in combination with a theory for damage accumulation such as the Palmgren–Miner rule. Cycle-counting requires the identification of load reversals or closed hysteresis loops, which can only be identified by considering the stress history. An alternative approach is to integrate a fatigue damage parameter in the time domain [1, 2, 3, 4], thus enabling fatigue life prediction based on an evolving stress state rather than a given stress history. Particularly, the continuous-time fatigue (CTF) model of Ottosen *et al.* [3], also referred to as the *continuum approach* to fatigue, emerges as a simple and versatile method, where the fatigue phenomenon is modeled as an evolution of state variables governed by rate-independent differential equations.

We consider the crack initiation stage of high-cycle fatigue (HCF) of an isotropic material subjected to a cyclic, multiaxial, nonproportional stress evolution. By HCF we mean a rate-independent fatigue process involving predominantly elastic deformations with more than 10^4 cycles to failure. The crack initiation stage of fatigue includes accumulation of permanent microstructural damage, followed by nucleation, growth and coalescence of microcracks into a dominant crack [5]. During this process, the microdamage is assumed to be spatially distributed with negligible effect on the constitutive behavior of the material. The experimentally observed fatigue life, as quantified by cycles to failure, is assumed to be dominated by this crack initiation stage. That is, the number of cycles spent in the subsequent stages of stable and unstable macroscopic crack propagation [5] is neglected.

The concept of the cycle is extremely useful in many fatigue applications. However, for general stress histories—which can be envisioned as directed paths in six-dimensional stress space—it is not obvious how to define cycles (see *e.g.* Refs. [6, 7, 8]). This problem is inherent to all cycle counting-based fatigue models. An important benefit of the CTF model of Ottosen *et al.* is that damage is integrated in the time domain without any need for identifying cycles, and that the method offers a unified treatment of uniaxial/multiaxial, proportional/nonproportinal and cyclic/noncyclic stress evolutions [3]. The possibility to treat general stress histories is pivotal to the industry trend towards integral structures, where large free-formed parts with nondistinct or varying stress paths replace assemblies of struts, bars and beams.

Ottosen and co-workers [3] formulated a CTF model inspired by kinematic hardening in plasticity [9]. This original formulation considers HCF in isotropic materials. It is based on the concept of an endurance surface centered at a deviatoric backstress, and an increasing, scalar variable representing damage. The evolution of the backstress and damage is governed by two ordinary differential equations (ODEs). This CTF model gives a good prediction of the Wöhler curves for AISI 4340 steel alloy for a range of the mean stress, and qualitatively captures the behavior of the fatigue limit for nonproportional stress [3].

Several modifications and extensions to the original CTF model have been proposed in the literature. Stress gradient effects were incorporated into the CTF model by Ottosen *et al.* [10]. This crucially enables automatic handling

*Corresponding author.

Email addresses: stefan.lindstroem@gmail.com (Stefan B. Lindström), carl-johan.thore@liu.se (Carl-Johan Thore), shyam.suresh@liu.se (Shyam Suresh), anders.klarbring@liu.se (Anders Klarbring)

of stress concentrations in complex geometries. Furthermore, Holopainen and co-workers [11, 12] formulated a CTF model for transversely isotropic materials, as well as a CTF model for anisotropic materials where the damage is modeled as a tensor field [13]. An extension to include low-cycle fatigue has also been proposed [14]. Brighenti *et al.* [15] suggested a more general expression for the endurance surface, and demonstrated fair agreement between modeled fatigue life and experimentally observed fatigue life for a range of steel alloys subjected to nonproportional stress. However, this could only be achieved by modifying the material parameters depending on the stress history, which implies that *predicting* fatigue for general stress histories is currently beyond the capability of the CTF model.

In this work, we reexamine the original CTF model of Ottosen *et al.* [3] to uncover fundamental properties of the model. We derive an analytical solution for the damage development due to proportional cyclic stress, including a closed-form expression for fatigue in simple shear. Also, we propose an acceleration scheme based on Wynn's epsilon algorithm [16] for cyclic loading. Finally, we investigate the mechanisms responsible for difficulties in predicting fatigue for nonproportional stress histories with this model. To this end, we investigate the fatigue predicted by the CTF model for 7050-T7451 aluminum alloy and AISI 4340 steel alloy subjected to different states of nonproportional stress.

2. Theory

Considering the postulated properties of HCF, neither the elastic constitutive behavior, nor the macroscale geometry is affected by damage until failure. Thus, we take the stress evolution $\boldsymbol{\sigma}(t)$ in a material point to be a given function of time in the fatigue analysis.

2.1. Governing equations

The fatigue model of Ottosen *et al.* [3] is based on the concept of an endurance surface $\{\boldsymbol{\sigma} \mid \beta(\boldsymbol{\sigma}, \boldsymbol{\alpha}) = 0\}$ defined by an endurance function β and a deviatoric backstress $\boldsymbol{\alpha}$. Damage development only occurs during onloading when $\beta > 0$ and $\dot{\beta} > 0$. The endurance function is taken to be [3]

$$\beta(\boldsymbol{\sigma}, \boldsymbol{\alpha}) = \frac{1}{S_\mathrm{e}} \left[\sigma_\mathrm{eff}(\boldsymbol{\sigma}, \boldsymbol{\alpha}) + A \operatorname{tr}(\boldsymbol{\sigma}) - S_\mathrm{e} \right], \tag{1}$$

where S_e is the endurance stress, A is a material constant, and $\operatorname{tr}(\boldsymbol{x})$ denotes the trace of a tensor $\boldsymbol{x}$. The effective stress σ_eff is based on the deviatoric stress $\boldsymbol{s} = \operatorname{dev}(\boldsymbol{\sigma})$, where $\operatorname{dev}(\boldsymbol{x}) = \boldsymbol{x} - \frac{1}{3}\operatorname{tr}(\boldsymbol{x})\boldsymbol{\delta}$ is the deviator of a tensor $\boldsymbol{x}$, and $\boldsymbol{\delta}$ is the unit tensor. Particularly, we have

$$\sigma_\mathrm{eff}(\boldsymbol{\sigma}, \boldsymbol{\alpha}) = \sqrt{\tfrac{3}{2}} \left\| \boldsymbol{s} - \boldsymbol{\alpha} \right\|, \tag{2}$$

where $\|\boldsymbol{x}\| = \sqrt{\boldsymbol{x} : \boldsymbol{x}}$ is the Frobenius norm induced by the Frobenius inner product $\boldsymbol{x} : \boldsymbol{y} = \operatorname{tr}(\boldsymbol{x}\boldsymbol{y}^\top)$ of second-order tensors $\boldsymbol{x}$ and $\boldsymbol{y}$. Thus, we may envisage the endurance surface as a cone with its axis intersecting $\boldsymbol{\alpha}$ while being parallel to the hydrostatic line in principal stress space (Fig. 1).

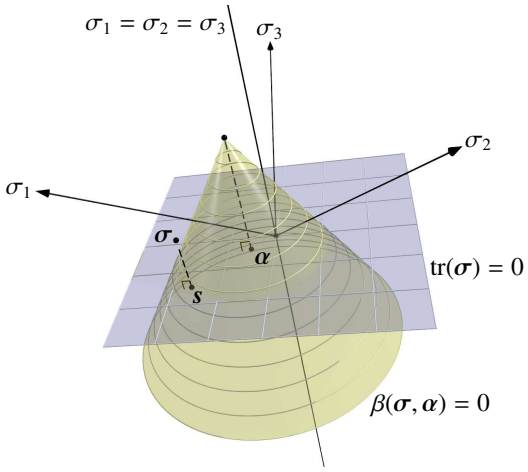

Figure 1: Endurance surface $\beta = 0$ (cone) and deviatoric plane $\operatorname{tr}(\boldsymbol{\sigma}) = 0$ (rectangle) in principal stress space.

The damage is represented by a scalar D, ranging from $D = 0$ for the undamaged material to a critical value $D = 1$, herein representing the damage at failure. The state variables $\boldsymbol{\alpha}$ and D are governed by the initial value problem (IVP) [3, 17]

$$\dot{\boldsymbol{\alpha}} = (\boldsymbol{s} - \boldsymbol{\alpha}) C H(\beta) H(\dot{\beta}) \dot{\beta}, \qquad \boldsymbol{\alpha}(0) = \boldsymbol{0}, \tag{3a}$$

$$\dot{D} = g(\beta) H(\beta) H(\dot{\beta}) \dot{\beta}, \qquad D(0) = 0, \tag{3b}$$

for almost every time $t \geq 0$. Here, $C > 0$ is a material constant, and g is some function such that $g(\beta) > 0$ whenever $\beta > 0$. A superposed dot denotes time-derivative, and H denotes the Heaviside step function. Note that there is no need to include a damage-dependent factor on the right-hand side of Eq. (3b), since that factor can be eliminated using a change of variables [17].

By time differentiation of Eq. (1), while using Eq. (2), we find that [10]

$$\begin{aligned} S_\mathrm{e} \dot{\beta} &= \sqrt{\tfrac{3}{2}} \frac{(\boldsymbol{s} - \boldsymbol{\alpha})}{\|\boldsymbol{s} - \boldsymbol{\alpha}\|} : \dot{\boldsymbol{s}} - \sqrt{\tfrac{3}{2}} \frac{(\boldsymbol{s} - \boldsymbol{\alpha})}{\|\boldsymbol{s} - \boldsymbol{\alpha}\|} : \dot{\boldsymbol{\alpha}} + A \operatorname{tr}(\dot{\boldsymbol{\sigma}}) \\ &= \sqrt{\tfrac{3}{2}} \frac{(\boldsymbol{s} - \boldsymbol{\alpha})}{\|\boldsymbol{s} - \boldsymbol{\alpha}\|} : \dot{\boldsymbol{s}} - \sqrt{\tfrac{3}{2}} \|\boldsymbol{s} - \boldsymbol{\alpha}\| C H(\beta) H(\dot{\beta}) \dot{\beta} + A \operatorname{tr}(\dot{\boldsymbol{\sigma}}), \end{aligned} \tag{4}$$

where Eq. (3a) was inserted. From Eq. (4), we have

$$\underbrace{\left[S_\mathrm{e} + \sqrt{\tfrac{3}{2}} C \|\boldsymbol{s} - \boldsymbol{\alpha}\| H(\beta) H(\dot{\beta}) \right]}_{>0} \dot{\beta} = \sqrt{\tfrac{3}{2}} \frac{(\boldsymbol{s} - \boldsymbol{\alpha})}{\|\boldsymbol{s} - \boldsymbol{\alpha}\|} : \dot{\boldsymbol{s}} + A \operatorname{tr}(\dot{\boldsymbol{\sigma}}), \tag{5}$$

and by defining a rate function

$$\nu(\boldsymbol{\sigma}, \dot{\boldsymbol{\sigma}}, \boldsymbol{\alpha}) = \frac{1}{S_\mathrm{e} + \sqrt{\frac{3}{2}} C \|\boldsymbol{s} - \boldsymbol{\alpha}\|} \left[\sqrt{\tfrac{3}{2}} \frac{(\boldsymbol{s} - \boldsymbol{\alpha})}{\|\boldsymbol{s} - \boldsymbol{\alpha}\|} : \dot{\boldsymbol{s}} + A \operatorname{tr}(\dot{\boldsymbol{\sigma}}) \right], \tag{6}$$

we find through inspection of Eq. (5) that $H(\nu) = H(\dot{\beta})$, and that $H(\dot{\beta})\dot{\beta} = H(\nu)\nu$. It is then possible to eliminate $\dot{\boldsymbol{\alpha}}$ from the right-hand side of the evolution Eqs. (3a) and (3b), giving

$$\dot{\boldsymbol{\alpha}} = (\boldsymbol{s} - \boldsymbol{\alpha}) C H(\beta) H(\nu) \nu, \qquad \boldsymbol{\alpha}(0) = \boldsymbol{0}, \tag{7a}$$

$$\dot{D} = g(\beta) H(\beta) H(\nu) \nu, \qquad D(0) = 0. \tag{7b}$$

There is a jump on the right-hand side of Eq. (7a) due to the factor $H(\beta)$. Thus, the uniqueness of its solution $\boldsymbol{\alpha}(t)$ can be questioned. We show, however, that the solution $\boldsymbol{\alpha}(t)$ is indeed unique for the special case of proportional stress in Appendix A, and assume that this uniqueness extends to cases of nonproportional stress. Then, it follows from standard theory that the solution to Eq. (7b) is unique.

By taking the trace of Eq. (7a), we obtain the IVP

$$\frac{\mathrm{d}}{\mathrm{d}t}\mathrm{tr}(\boldsymbol{\alpha}) = -\mathrm{tr}(\boldsymbol{\alpha})CH(\beta)H(\nu)\nu, \qquad \mathrm{tr}[\boldsymbol{\alpha}(0)] = 0, \tag{8}$$

It is readily confirmed that $\mathrm{tr}(\boldsymbol{\alpha}) = 0$, $t \geq 0$, solves this problem. Thus, the solution to Eq. (7a) remains deviatoric, as required.

2.2. Periodic, proportional stress

For the CTF model, it has been previously demonstrated for a periodic tensile/compressive cyclic stress, that the incremental damage per cycle in the steady-state can be expressed in terms of the maximum and minimum applied stress [3, 15]. Below, we extend this result to all periodic, proportional stress histories.

For a periodic, proportional stress the stress tensor can be expressed as

$$\boldsymbol{\sigma} = S(t)\boldsymbol{e}, \tag{9}$$

where $\boldsymbol{e}$ is a constant tensor such that $\|\boldsymbol{e}\| = 1$, $\mathrm{tr}(\boldsymbol{e}) \geq 0$, and $S(t) = \boldsymbol{\sigma} : \boldsymbol{e}$. The deviatoric stress is

$$\boldsymbol{s} = S(t)\mathrm{dev}(\boldsymbol{e}). \tag{10}$$

For some function $\alpha(t)$, we can express the backstress as (Appendix B)

$$\boldsymbol{\alpha} = \alpha(t)\mathrm{dev}(\boldsymbol{e}) + \boldsymbol{\alpha}_\perp(t), \tag{11}$$

where $\boldsymbol{\alpha}_\perp$ is deviatoric and orthogonal to $\mathrm{dev}(\boldsymbol{e})$ in the sense that $\mathrm{dev}(\boldsymbol{e}) : \boldsymbol{\alpha}_\perp = 0$. Inserting Eqs. (10) and (11) into Eq. (7a) yields

$$\dot{\alpha}\,\mathrm{dev}(\boldsymbol{e}) + \dot{\boldsymbol{\alpha}}_\perp = [(S-\alpha)\mathrm{dev}(\boldsymbol{e}) - \boldsymbol{\alpha}_\perp]\,CH(\beta)H(\nu)\nu, \tag{12}$$

with $\alpha(0) = 0$ and $\boldsymbol{\alpha}_\perp(0) = \boldsymbol{0}$. By identifying terms orthogonal to $\mathrm{dev}(\boldsymbol{e})$ in Eq. (12), we obtain

$$\dot{\boldsymbol{\alpha}}_\perp = -\boldsymbol{\alpha}_\perp CH(\beta)H(\nu)\nu, \qquad \boldsymbol{\alpha}_\perp(0) = \boldsymbol{0}. \tag{13}$$

We confirm that $\boldsymbol{\alpha}_\perp = \boldsymbol{0}$, $t \geq 0$, solves this IVP. Consequently, the backstress is reduced to

$$\boldsymbol{\alpha} = \alpha(t)\mathrm{dev}(\boldsymbol{e}), \tag{14}$$

so that we now only need to determine $\alpha(t)$.

The analytical solution for the steady-state backstress evolution is obtained by solving evolution Eq. (3a) specialized for proportional stress. Inserting Eqs. (10) and (14) into Eq. (2) yields

$$\sigma_{\mathrm{eff}}(S,\alpha) = \gamma|S-\alpha|, \qquad \gamma = \sqrt{\tfrac{3}{2} - \tfrac{1}{2}\mathrm{tr}(\boldsymbol{e})^2}, \tag{15}$$

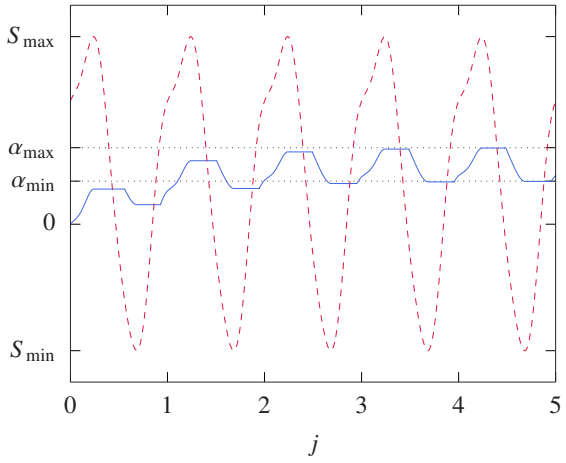

Figure 2: Sample evolution of the backstress α (solid line) for a periodic uniaxial stress (dashed line), showing cycles $j = 1, 2, \ldots$ For this particular case, $\dot{S}$ changes sign two times per cycle. The dotted lines indicate the analytical solution for $\alpha_{\min}$ and $\alpha_{\max}$.

where we used that $\mathrm{dev}(\boldsymbol{e}) : \mathrm{dev}(\boldsymbol{e}) = 1 - \frac{1}{3}\mathrm{tr}(\boldsymbol{e})^2$. Thus, the endurance function of Eq. (1) and its derivative become

$$\beta = \frac{1}{S_{\mathrm{e}}}\left(\gamma|S-\alpha| + A'S - S_{\mathrm{e}}\right), \tag{16a}$$

$$\dot{\beta} = \frac{1}{S_{\mathrm{e}}}\left[\gamma\,\mathrm{sgn}(S-\alpha)(\dot{S}-\dot{\alpha}) + A'\dot{S}\right], \tag{16b}$$

respectively, where $A' = A\,\mathrm{tr}(\boldsymbol{e}) > 0$ is introduced for convenience, and $\mathrm{sgn}(x)$ is the sign function. Inserting Eqs. (10), (14), (16a) and (16b) into Eq. (3a) yields

$$\dot{\alpha} = \frac{C}{S_{\mathrm{e}}}\left[\gamma\,\mathrm{sgn}(S-\alpha)(\dot{S}-\dot{\alpha}) + A'\dot{S}\right](S-\alpha)H(\beta)H(\dot{\beta}). \tag{17}$$

With the additional requirements that $\dot{S}$ shifts sign exactly two times each cycle, Eq. (17) can be integrated analytically using the same method as for the uniaxial case presented in Ref. [3]. The details are found in Appendix C. Thus, the maximum and minimum of $\alpha(t)$ during a cycle are obtained as functions of the maximum and minimum of $S(t)$: $\alpha_{\max} = \alpha_{\max}(S_{\max}, S_{\min})$ and $\alpha_{\min} = \alpha_{\min}(S_{\max}, S_{\min})$.

A sample evolution of the backstress, integrated using IVP (7a) for a cyclic uniaxial applied stress, is plotted in Fig. 2, where the analytically obtained values for $\alpha_{\min}$ and $\alpha_{\max}$ from Appendix C are indicated by tick marks. The explicit fourth order Dormand–Prince method (`ode45` in Octave [18]) is used for integrating IVPs. The backstress exhibits a transient, and then evolves into a steady-state cyclic behavior. This transient is interpreted as a manifestation of localized inelastic deformations associated with damage development inside the matrix of grains dominated by elastic deformation, *cf.* introduction of Ref. [3].

The fatigue limit for cyclic, proportional stress is obtained by requiring that $\beta(S_{\min}, \alpha_\infty) = 0$ and $\beta(S_{\max}, \alpha_\infty) = 0$ in Eq.

(16a), for some unknown backstress $\alpha_\infty \in (S_{\min}, S_{\max})$. That is,

$$0 = \frac{1}{S_e}\left[\gamma(S_{\max} - \alpha_\infty) + A' S_{\max} - S_e\right], \tag{18a}$$

$$0 = \frac{1}{S_e}\left[-\gamma(S_{\min} - \alpha_\infty) + A' S_{\min} - S_e\right]. \tag{18b}$$

By eliminating α_∞ and introducing the effective stress amplitude $\sigma_a = \frac{\gamma}{2}(S_{\max} - S_{\min})$ and the effective mean stress $\sigma_m = \frac{1}{2}(S_{\max} + S_{\min})$, we find that

$$\sigma_a = S_e - A'\sigma_m. \tag{19}$$

At the fatigue limit, the amplitude of the cyclic stress depends linearly on the mean stress, which is commonly depicted using a Haigh diagram.

In the particular case of uniaxial tension/compression $\sigma(t)$, we have $S(t) = \sigma(t)$, $\mathrm{tr}(\boldsymbol{e}) = 1$ and $\gamma = 1$, so that the effective stress amplitude $\sigma_a = (\sigma_{\max} - \sigma_{\min})/2$ is equal to the actual amplitude of $\sigma(t)$. In the case of simple shear $\tau(t)$, we have $S(t) = \sqrt{2}\,\tau(t)$, $\mathrm{tr}(\boldsymbol{e}) = 0$ and $\gamma = \sqrt{3/2}$, which gives an effective stress amplitude $\sigma_a = \sqrt{3}(\tau_{\max} - \tau_{\min})/2$ consistent with the von Mises effective stress amplitude. In Appendix C, we also obtain closed-form expressions for $\alpha_{\max}(S_{\max}, S_{\min})$ and $\alpha_{\max}(S_{\max}, S_{\min})$ in the case of simple shear.

As observed in Sect. 2.2 and Fig. 2, periodic proportional stress leads to a steady-state cyclic evolution of the backstress $\alpha(t)$. Then, by integration of Eq. (3b) over one cycle of the steady-state, following the method of Ottosen *et al.* [3], the incremental damage per cycle becomes

$$\begin{aligned}\Delta D = {} & G\{\beta[S_{\min}, \alpha_{\min}(S_{\max}, S_{\min})]\} \\ & + G\{\beta[S_{\max}, \alpha_{\max}(S_{\max}, S_{\min})]\},\end{aligned} \tag{20}$$

where $G(\beta) = \int_0^\beta g(\beta')\mathrm{d}\beta'$, and the function $\beta(S, \alpha)$ refers to Eq. (16a). This demonstrates that $\Delta D = \Delta D(S_{\max}, S_{\min})$ for periodic, proportional stress, provided that $\dot{S}$ shifts sign exactly two times each cycle. Hence, it is possible to express the fatigue criterion in terms of a stress constraint:

$$N_f \Delta D(S_{\max}, S_{\min}) < 1, \tag{21}$$

with N_f the number of cycles to failure. Here, we have neglected effects of the transient (Fig. 2), understanding that the damage accumulated in the steady-state dominates HCF.

2.3. Damage sequence acceleration

Integrating the full stress history of the material across the large number of cycles in HCF leads to a great computational cost. Whenever a steady-state exists, this computational cost can be reduced using extrapolation. Further improvements may be gained by employing some method of acceleration.

For a cyclic applied stress of period T, let $D_j = D(jT)$, $j = 0, 1, 2, \ldots$ be the damage after the jth cycle, as obtained by integration. The incremental damage between cycles is $\Delta D_j = \frac{1}{2}(D_{j+1} - D_{j-1})$. If a steady-state exists, we have $\Delta D_j \to \Delta D$ when $j \to \infty$, for some constant value ΔD. Moreover, if $\{\Delta D_j\}_{j=1}^\infty$ is a converging sequence, it may be accelerated by standard sequence acceleration methods.

Herein, we apply Wynn's epsilon algorithm to the truncated sequence $\{\Delta D_j\}_{j=1}^n$. This recursive method is formulated as: [16]

$$\epsilon_{-1}^{(j)} = 0, \qquad j = 1, 2, \ldots, n, \tag{22a}$$

$$\epsilon_0^{(j)} = \Delta D_j, \qquad j = 1, 2, \ldots, n, \tag{22b}$$

$$\epsilon_{k+1}^{(j)} = \epsilon_{k-1}^{(j+1)} + \frac{1}{\epsilon_k^{(j+1)} - \epsilon_k^{(j)}}, \qquad \begin{cases} k = 1, \ldots, n-1, \\ j = 1, \ldots, n-k, \end{cases} \tag{22c}$$

where $\epsilon_{2k}^{(n-2k)}$, $k = 1, 2, \ldots, \left\lfloor \frac{n-1}{2} \right\rfloor$ provides increasingly better approximations for ΔD. That is, only elements with even subscripts approximate ΔD. We obtain the accumulated damage after $N \gg n$ cycles by linear extrapolation:

$$D_N = D_n + (N - n)\epsilon_{2k}^{(n-2k)}, \qquad k = \left\lfloor \frac{n-1}{2} \right\rfloor. \tag{23}$$

3. Results and Discussion

We proceed to numerically investigate the properties of the fatigue model in the context of periodic, biaxial, nonproportional stress. For this, we choose the same function

$$g(\beta) = K e^{L\beta}, \tag{24}$$

as in Refs. [3, 10], where $K > 0$ and $L > 0$ are nondimensional material parameters. First, however, the parameters of the model are fit to uniaxial experimental data.

3.1. Parameter fit to uniaxial test

The CTF model has five material parameters, S_e, A, C, K and L, which we fit to experimental fatigue data in the literature for 7050-T7451 aluminum alloy [19], as well as AISI 4340 tempered to 1380 MPA ultimate stress [19]. In those experiments, unnotched, cylindrical test specimens were subjected to cyclic stress in tension/compression at room temperature. The number of cycles to failure N_f at different stress amplitudes σ_a and stress ratios R were reported as triplets $(N_{fi}, \sigma_{ai}, R_i)$, $i = 1, 2, \ldots, n_s$. We digitized the experimental data using the Engauge Digitizer Software [20].

The fatigue model is fit to the n_s data points by minimizing a sum of squared errors,

$$\min_{\substack{S_e \geq 0, \\ A \geq 0, C \geq 0, \\ K \geq 0, L \geq 0}} \sum_{i=1}^{n_s} \left[\sigma_a(N_{fi}, R_i; S_e, A, C, K, L) - \sigma_{ai}\right]^2, \tag{25}$$

where $\sigma_a(N_f, R; S_e, A, C, K, L)$ is the numerically obtained model prediction of the stress amplitude. A BFGS quasi-Newton optimization algorithm (`fminunc` in Octave [18]) yields a fair fit to the experimental data for 7050-T7451 (Fig. 3) and AISI 4340 (Fig. 4), with parameters as compiled in Table 1. The standard deviation of $\log_{10}(\sigma_{ai}) - \log_{10}(\sigma_a)$ is 0.0562 and 0.0243, respectively, for 7050-T7451 and AISI 4340 (insets of Figs. 3 and 4).

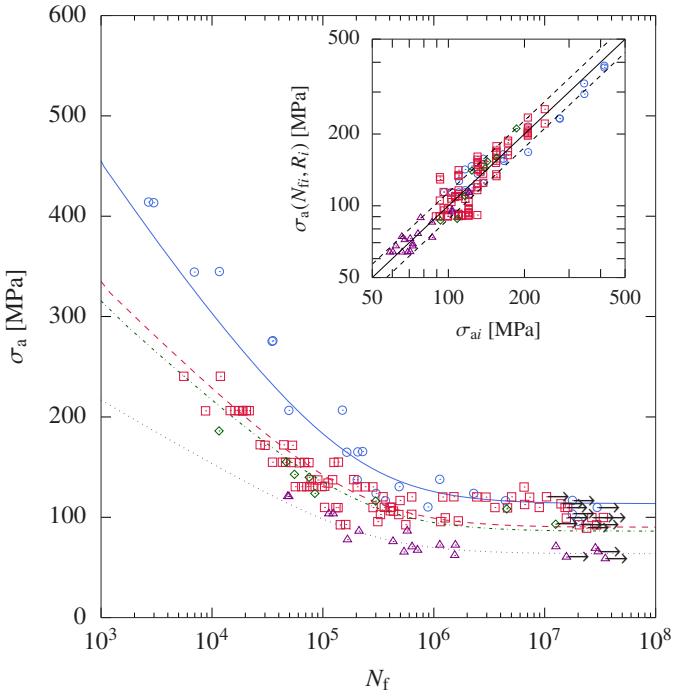

Figure 3: Parameter fit for 7050-T7451 aluminum alloy. The lines represent the model fit while the scatter data points are measurements conducted at different stress ratios: $R = -1$ (circles, solid line), $R = 0$ (squares, dashed line), $R = 0.1$ (diamonds, dash-dotted line) and $R = 0.5$ (triangles, dotted line). Arrows indicate runout. In the inset, the predicted stress amplitude $\sigma_a(N_{fi}, R_i)$ for each measured life N_{fi} is plotted against measured stress amplitude σ_{ai}. The dashed lines indicate one standard deviation (0.0562) of the logarithm of σ_a.

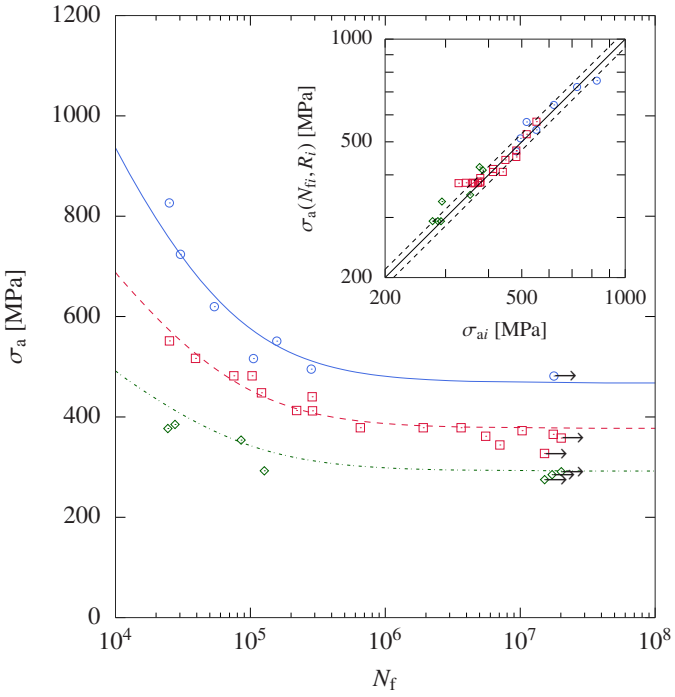

Figure 4: Parameter fit for AISI 4340 steel alloy. The lines represent the model fit while the scatter data points are measurements conducted at different stress ratios: $R = -1$ (circles, solid line), $R = 0$ (squares, dashed line) and $R = 0.43$ (triangles, dotted line). Arrows indicate runout. In the inset, the predicted stress amplitude $\sigma_a(N_{fi}, R_i)$ for each measured life N_{fi} is plotted against measured stress amplitude σ_{ai}. The dashed lines indicate one standard deviation (0.0243) of the logarithm of σ_a.

Material	S_e [MPa]	A	C	K [10^{-6}]	L
7050-T7451	113.3	0.2611	0.5039	5.111	2.556
AISI 4340	467.8	0.2397	3.023	41.70	4.967

Table 1: Fatigue parameters for 7050-T7451 aluminum alloy corresponding to the fit in Fig. 3, and for AISI 4340 steel alloy corresponding to the fit in Fig. 4.

3.2. *Biaxial, nonproportional stress*

A fair predictive capability can be expected in the range of proportional stresses spanned by the experiments to which the CTF model is fit. From previous investigations, the model also predicts the endurance limit for nonproportional load cases [3]. The question remains whether the CTF model, at least qualitatively, predicts the fatigue life for nonproportional stresses. The response to nonproportional stress was investigated for both 7050-T7451 and AISI 4340, but since no remarkable qualitative differences were observed between those materials, we only report the details for 7050-T7451 aluminum alloy below.

Biaxial, nonproportional testing is often conducted using thin-walled cylinder specimens, subjected to elongation and torsion, see *e.g.* Ref. [21]. Thus, we consider a combination of tension/compression and simple shear, fluctuating with zero mean stress at a constant angular frequency ω:

$$\sigma_{11} = \frac{\sigma_0}{\sqrt{2}\cos\frac{\psi}{2}}\sin(\omega t), \tag{26a}$$

$$\sigma_{12} = \frac{\sigma_0}{\sqrt{6}\cos\frac{\psi}{2}}\sin(\omega t + \psi), \tag{26b}$$

$$\sigma_{22} = \sigma_{33} = \sigma_{13} = \sigma_{23} = 0, \tag{26c}$$

where $\sigma_0 > 0$ is a constant, and $\psi \in [0, \frac{\pi}{2}]$ is the phase difference between tension and simple shear. An in-phase (IP) stress state is obtained for $\psi = 0$. For this IP stress fluctuation, the effective stress amplitude is $\sigma_a = \sigma_0$ according to the framework in Sect. 2.2. We also consider out-of-phase (OP), nonproportional stress fluctuations with $\psi > 0$. Note that the phase dependence of the amplitudes of σ_{11} and σ_{12} is chosen to ensure that the maximum von Mises-equivalent stress reversal takes the same value σ_0 for all values of ψ. Thus, the OP stress paths pass through the extrema of the IP stress path (Fig. 5a). Also, this ensures that all stress paths have the same minimum circumscribed circle (MCC, see Ref. [22]) in deviatoric stress space, where the 90° OP stress traces this MCC exactly (Fig. 5b). This makes the stress paths comparable in a von Mises sense.

For IP and 60° OP stress, the damage develops similarly to a staircase function, at an angular frequency of 2ω, which derives from the applied stress (Fig. 6a). After a transient, the backstress of IP and 60° OP stress develop into repeating cycles in

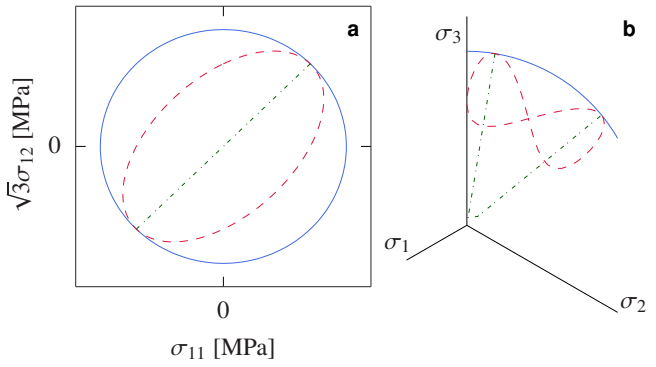

Figure 5: **a** Stress variation for tension combined with simple shear of different phase difference: IP (dash-dotted line), 60° OP (dashed line) and 90° OP (solid line). **b** The same paths in the deviatoric plane.

the deviatoric plane (Fig. 6b). However, for 90° OP stress the damage develops at an angular frequency that does not appear to have any simple relation to the applied angular frequency (Fig. 6a), and the path of the backstress describes a spiral with multiple cusps. Eventually, this spiral narrows towards a stationary point (Fig. 6b). The cusps in the path of the backstress for 90° OP are due to the nonlinearity created by the step functions in the evolution Eq. (3a), which intermittently arrests the evolution of the backstress.

To further investigate this unexpected behavior of the governing ODEs, we integrate for 300 cycles with $\sigma_0 = 150\,\text{MPa}$ and $\psi = \{0°, 60°, 90°\}$. The beginning of the sequence $\{\Delta D_j\}_{j=1}^{\infty}$ of damage increments per cycle is illustrated in Fig. 6c, showing convergence for IP and 60° OP after a few cycles, contrasted by a prolonged transient for 90° OP. We also plot the magnitude of the relative difference between the incremental damage and the approximated steady-state incremental damage $\Delta D \approx \Delta D_{300}$ (Fig. 6d). This difference diminishes to a noise floor for all cases, demonstrating the existence of a steady-state.

Stress-controlled fatigue experiments including OP stress fluctuations are scarce in the literature. However, strain-controlled nonproportional fatigue tests of 7075-T651 aluminum alloy tubular specimens have been reported for the HCF regime [21]. These experiments show that OP stress fluctuations *shorten* fatigue life, as compared to the IP case [21]. The linear elastic material behavior during the crack initiation phase, and our assumption that crack initiation dominates fatigue life in the HCF regime, imply that OP stress fluctuations also shorten fatigue life in stress-controlled HCF. The behavior for a range of steel alloys is qualitatively similar [23, 24]. With the present model and with $\sigma_0 = 150\,\text{MPa}$ and 90° OP, however, the damage per cycle in the steady-state is a factor 4 smaller than the damage increment per cycle for IP stress, which is irreconcilable with experiments.

3.3. Rotary stress

For a rotary stress state, the invariants of the stress tensor remain constant while the principal stress directions vary. As a result, each plane through the material experiences stress reversals so that fatigue damage is to be expected. Fatigue models based solely on stress invariants will necessarily fail to predict any damage. Critical plane models, on the other hand, consider the fluctuations of the traction vector on each plane of the material [25, 26], and thus capture the stress reversals for rotary stress states. The critical plane models are computationally expensive due to the maximization of fatigue across all planes and points in the material [27, 26], which is avoided in the CTF model.

For the CTF model, we consider a rotating state of simple shear stress with stationary principal stresses $\pm\sigma_0/\sqrt{3}$ and 0:

$$\sigma_{11} = -\sigma_{22} = \frac{\sigma_0}{\sqrt{3}}\cos(\omega t), \tag{27a}$$

$$\sigma_{12} = \frac{\sigma_0}{\sqrt{3}}\sin(\omega t), \tag{27b}$$

$$\sigma_{33} = \sigma_{13} = \sigma_{23} = 0. \tag{27c}$$

This applied stress, which may be difficult to achieve experimentally, corresponds to circular path in deviatoric stress space with $\text{tr}(\boldsymbol{\sigma}) = 0$. Its geometrical simplicity makes it suitable for identifying the reason for the misprediction of fatigue life for nonproportional stress (Sect. 3.2).

The damage development of the rotary stress state in Eqs. 27a through (27c) is compared to fully reversed shear with the same magnitude, that is, with $\sigma_{12} = \frac{\sigma_0}{\sqrt{3}}\sin(\omega t)$ and all other stress components zero. The rotary stress states display a damage development similar to that of the 90° OP case: The damage per cycle decreases and becomes very small as compared to the damage per cycle in the corresponding proportional case of fully reversed shear (Fig. 7a). Also, while the backstress of the proportional case displays cyclic behavior, the backstress of the rotary stress spirals around the point $\boldsymbol{\alpha} = \mathbf{0}$ on a path with cusps corresponding to intermittent arrested states (Fig. 7b).

Although planes in the material experiences full stress reversals for the rotary stress state, the CTF model predicts much less damage for the rotary stress than for proportional stress. We believe that this is a misprediction of the model due to its failure to predict damage when the stress moves tangentially to the endurance surface.

3.4. Damage sequence acceleration

As observed above, the sequence $\{\Delta D_j\}_{j=1}^{\infty}$ converges to a limiting ΔD, at least for proportional stress or nonproportional stress with a moderate phase difference. For these instances of convergence, that is when ΔD exists, it is possible to accelerate the sequence using standard methods. Herein, we evaluate the effectiveness of Wynn's epsilon algorithm for the combination of tension/compression and simple shear with $\psi = \{0°, 60°\}$ and $\sigma_0 = 150\,\text{MPa}$.

In the case of IP stress, the magnitude of the relative difference between the incremental damage and the approximated steady-state incremental damage diminishes exponentially to the noise floor in ten cycles (Fig. 8a). Wynn's epsilon algorithm accelerates this sequence of incremental damage, so that only five to six cycles are needed to reach the noise floor (Fig. 8a). For OP stress with $\psi = 60°$ the rate of convergence is impaired. Wynn's epsilon algorithm improves the rate of convergence, but not as efficiently as for the proportional IP stress case.

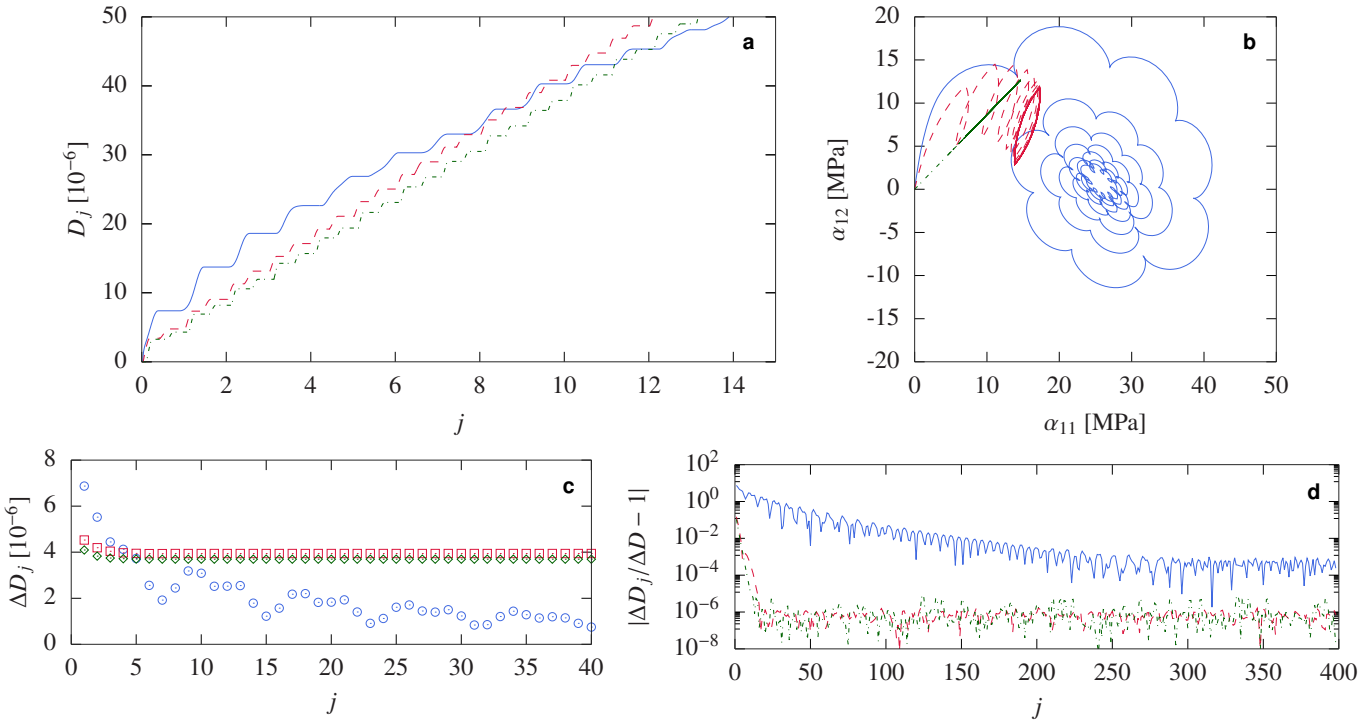

Figure 6: Cyclic stress fatigue for 7050-T7451 aluminum alloy. **a** Damage development in the cases of IP (dash-dotted line), 60° OP (dashed line) and 90° OP (solid line) stress variation for tension combined with simple shear, and $\sigma_0 = 150$ MPa. **b** The development of backstress for the first 60 cycles of stress. **c** Incremental damage against cycle number for $\sigma_0 = 150$ MPa in the cases of IP (diamonds), 60° OP (squares) and 90° OP (circles). **d** Development of relative difference to steady-state damage per cycle.

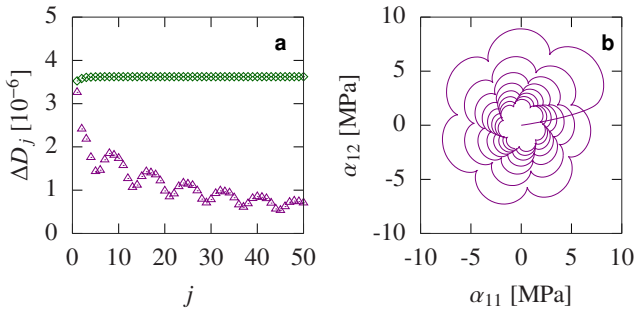

Figure 7: **a** Incremental damage against cycle number for 7050-T7451 aluminum alloy with $\sigma_0 = 150$ MPa in the cases of fully reversed shear (diamonds) and rotary simple shear (triangles) . **b** The development of backstress for the first 60 cycles of rotary simple shear.

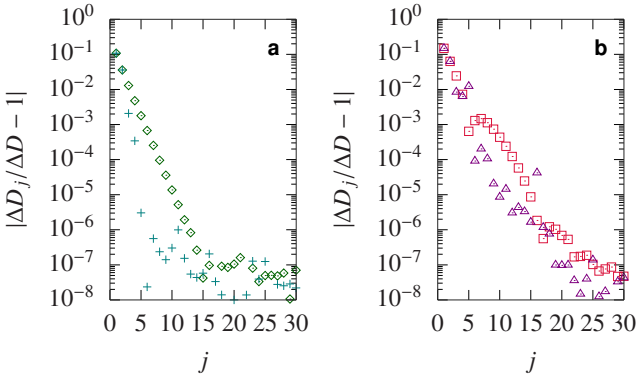

Figure 8: Development of relative difference to steady-state damage per cycle for 7050-T7451 aluminum alloy with $\sigma_0 = 150$ MPa and **a** $\psi = 0°$ (diamonds) and corresponding accelerated sequence (plus symbols), and **b** $\psi = 60°$ (squares) and corresponding accelerated sequence (triangles).

4. Conclusions

For proportional, cyclic stress, which shifts sign exactly two times each cycle, the CTF model can be integrated analytically to yield the damage per cycle in the steady-state. Particularly, the damage per cycle can be written on closed form for the case of simple shear. In numerical simulations, the damage per cycle converges exponentially to a constant value.

The CTF model gives a fair fit to the Wöhler curves of 7050-T7451 high-strength aluminum alloy. This fit has a standard deviation of 0.0517 in the base-10 logarithm of the stress amplitude. The same conclusion is drawn for AISI 4340 steel alloy, with a standard deviation of 0.0243.

For a combination of cyclic, tensile/compressive and shear stress, with a moderate phase difference, the CTF model predicts a constant damage per cycle, and a fatigue life close to that of proportional cyclic loading of the same effective stress amplitude. Moreover, in cases of proportional, cyclic stress, or for nonproportional stress with a moderate phase angle, Wynn's epsilon algorithm can be used to accelerate the sequence of damage increment per cycle. This can be useful for reducing the computational effort for complicated cyclic stress histories.

For a rotary stress state of simple shear, or for a combination

of cyclic, tensile/compressive and shear stress with a 90° phase difference, the CTF model exhibits an extended transient with intermittent arrested states . The predicted fatigue life is four times that of a proportional cyclic stress with the same effective stress amplitude. This contrasts experiments in the literature that demonstrate a reduced fatigue life for nonproportional stress [21]. We observe that the problems with arrested states appear for stress paths that are tangential to the endurance surface, which is particularly clear for rotary simple shear (Fig. 7). Hence, a remedy is likely to be found by modifying the governing ODEs to produce a nonzero damage increment for such tangential stress paths.

The CTF model investigated herein has many virtues, which we further establish by demonstrating uniqueness and new analytical solutions for proportional, cyclic stress. However, to use the CTF model in practice for predicting the fatigue life of, *e.g.*, integral metallic structures subjected to multiple out-of-phase loads across a wide frequency range, it is necessary to ensure that the prediction is at least conservative for every conceivable load. As demonstrated above, further development of the model to address the issues observed for nonproportional and rotary stress is needed. We hope to be able to develop a gently modified CTF model that addresses these issues in the future.

Acknowledgments

This work was performed within the AddMan project, funded by the Clean Sky 2 joint undertaking under the European Unions Horizon 2020 research and innovation program [grant number 738002], and within the Center for Additive Manufacturing-Metal (CAM 2) financed by Sweden's innovation agency [grant number 2016-05175].

Appendix A. Uniqueness of evolution for proportional stress

For a proportional stress, Eq. (9), we use the framework in Sect. 2.2 with Eqs. (1), (2), (6) and (7a) to obtain the ODE

$$\dot{\alpha} = (S - \alpha) C H(\beta) H(\nu) \nu, \tag{A.1}$$

with $\beta = \beta(S, \alpha)$ according to Eq. (16a) and

$$\nu = \frac{\gamma \operatorname{sgn}(S - \alpha) + A'}{S_\mathrm{e} + C\gamma|S - \alpha|} \dot{S}, \tag{A.2}$$

where we recall that $1 \leq \gamma \leq \sqrt{3/2}$ and $A' \geq 0$. For realistic materials, we must have $A' < \gamma$ to ensure that $\nu > 0$ during onloading in the case $\{S - \alpha < 0 \ \wedge \ \dot{S} < 0\}$. The right-hand side of Eq. (A.1) has a discontinuity in α at $\beta(S, \alpha) = 0$ due to the $H(\beta)$ factor. Consequently, the standard requirement of Lipschitz continuity for uniqueness of solution is not fulfilled.

Consider the general framework of a one-dimensional ODE

$$\dot{x} = f(x, t), \qquad t \in \mathbb{R}, \tag{A.3}$$

where f may be discontinuous in the first variable at fixed isolated points. A continuous function $x(t)$ that satisfies Eq. (A.3), except at isolated points where $\dot{x}$ may not be defined, is called a solution of Eq. (A.3). We are interested in conditions for *right uniqueness* [28] of such solutions, where right uniqueness means that every two solutions satisfying $x(t_0) = x^*$ for a given x^* coincide on a closed time interval $t_0 \leq t \leq t_1$. For x^* being a point of discontinuity of f, let $f^+(x^*, t)$ and $f^-(x^*, t)$ denote limits of $f(x, t)$ from the right and left w.r.t. x, respectively. If $f^+(x^*, t) > 0$ and $f^-(x^*, t) < 0$, then a solution $x(t)$ of Eq. (A.3) starting at x^* is non-unique since, loosely speaking, $\dot{x}$ can take any of the values $f^+(x^*, t)$ or $f^-(x^*, t)$, and arbitrarily move the solution to the right or to the left. On the other hand, when both of the limits have the same sign, under some further smoothness assumptions for f, a solution can be shown to be right unique. Even less restrictive, Theorem 2, page 110, in Filippov [28] shows that right uniqueness holds, under additional smoothness assumptions, if one of the inequalities $f^+(x^*, t) < 0$ or $f^-(x^*, t) > 0$ are satisfied.

Given these facts we consider Eq. (A.1). Introducing $\kappa = \operatorname{sgn}(S - \alpha)$ in Eq. (16a) gives

$$S_\mathrm{e} \beta = \kappa\gamma(S - \alpha) + A'S - S_\mathrm{e}. \tag{A.4}$$

Depending on the value of κ, we then make a change-of-variable

$$x_\kappa = \kappa\gamma(S - \alpha) + A'S - S_\mathrm{e}, \tag{A.5}$$

so that $\beta = x_\kappa / S_\mathrm{e}$, $H(\beta) = H(x_\kappa)$ and $x_\kappa = x_\kappa^* = 0$ is a possible discontinuity point. This point is fixed in the new variable x_κ meaning that when Eq. (A.1) is rewritten in this variable, the theorem of Filippov, cited above, applies. Using Eq. (A.5), Eq. (A.1) becomes

$$\dot{x}_\kappa = f_\kappa(x_\kappa, t) = (\kappa\gamma + A')\dot{S} - \kappa\gamma[S - \alpha(x_\kappa)] C H(x_\kappa) H(\nu_\kappa) \nu_\kappa, \tag{A.6}$$

with

$$\nu_\kappa = \frac{(\kappa\gamma + A')\dot{S}}{S_\mathrm{e} + C\gamma|S - \alpha(x_\kappa)|}. \tag{A.7}$$

We identify the following mutually excluding cases:

I. $(\kappa\gamma + A')\dot{S} = 0$: Eq. (A.7) gives $\nu_\kappa = 0$ and, furthermore, Eq. (A.6) gives $\dot{x}_\kappa = 0$, thus ensuring uniqueness.

II. $(\kappa\gamma + A')\dot{S} < 0$: Eq. (A.7) implies that $\nu_\kappa < 0$ so that $\dot{x}_\kappa = (\kappa\gamma + A')\dot{S}$, ensuring uniqueness.

III. $(\kappa\gamma + A')\dot{S} > 0$: From Eq. (A.6), we have $f_\kappa^-(0, t) = (\kappa\gamma + A')\dot{S} > 0$, so that uniqueness is ensured by the theorem of Filippov at the possible discontinuity point $x_\kappa = x_\kappa^* = 0$.

Since the cases I, II and III cover all possible situations, uniqueness is ensured for the solution of Eq. (A.1).

Appendix B. Orthogonality in deviatoric tensor space

Let V_dev denote the set of deviatoric, symmetric tensors, that is

$$V_\mathrm{dev} = \{\boldsymbol{x} \in \mathbb{R}^{3\times3} \mid \boldsymbol{x} = \boldsymbol{x}^\top, \operatorname{tr}(\boldsymbol{x}) = 0\}. \tag{B.1}$$

For a symmetric tensor $\boldsymbol{e}$, we introduce the subspace

$$V_\parallel = \{x \operatorname{dev}(\boldsymbol{e}) \mid x \in \mathbb{R}\}, \tag{B.2}$$

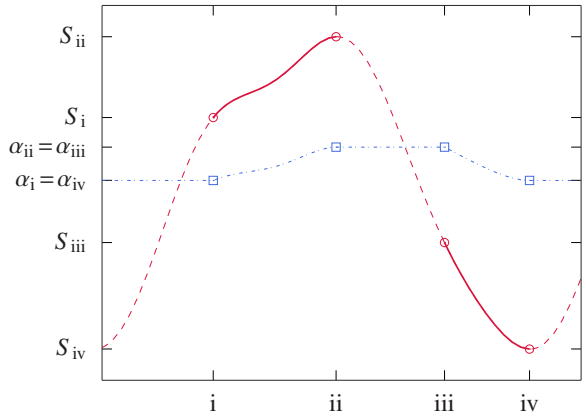

Figure C.9: Proportional, cyclic loading in the steady-state. Solid lines indicate $S(t)$ when $\beta \geq 0$, while dashed lines indicate $S(t)$ when $\beta < 0$. The dash-dotted line represents $\alpha(t)$. Damage development occurs from state (i) to state (ii), and from state (iii) to state (iv).

and its orthogonal complement

$$V_\perp = \{\boldsymbol{x}_\perp \mid \boldsymbol{x}_\perp : \boldsymbol{x}_\parallel = 0, \forall \boldsymbol{x}_\parallel \in V_\parallel\}. \tag{B.3}$$

Then, since V_{dev} is a Hilbert space, the Projection theorem asserts that every $\boldsymbol{x} \in V_{\text{dev}}$ can be uniquely decomposed as

$$\boldsymbol{x} = x\,\text{dev}(\boldsymbol{e}) + \boldsymbol{x}_\perp, \qquad x \in \mathbb{R},\ \boldsymbol{x}_\perp \in V_\perp. \tag{B.4}$$

Appendix C. Analytical solution for proportional stress

We define $\kappa = \text{sgn}(S - \alpha)$, so that $|S - \alpha| = \kappa(S - \alpha)$. The backstress evolution Eq. (17) for proportional stress becomes

$$\dot{\alpha} = \frac{C}{S_e}[\kappa\gamma(\dot{S} - \dot{\alpha}) + A'\dot{S}](S - \alpha)H(\beta)H(\dot{\beta}), \tag{C.1}$$

where β and $\dot{\beta}$ are given by Eqs. (16a) and (16b), respectively. As pointed out in Appendix A, it is required that $A' < \gamma$ for realistic materials.

For a cyclic, proportional stress such that $\dot{S}$ changes sign exactly two times each cycle, and with an amplitude sufficiently large to create fatigue, we assume that $\alpha(t)$ develops into a cyclic steady-state (Fig. 2). Following Ref. [3], we define state (i) as the point in a cycle when $\beta = 0$, $\dot{\beta} > 0$ and $\dot{S} > 0$, state (ii) when S reaches its maximum, state (iii) when $\beta = 0$, $\dot{\beta} > 0$ and $\dot{S} < 0$, and state (iv) when S reaches its minimum (Fig. C.9). From this scenario, we have $\alpha_i = \alpha_{iv}$, $\alpha_{iii} = \alpha_{ii}$, and we know that states (i) and (iii) are on the endurance surface, so that Eq. (16a) gives

$$S_i = \frac{S_e + \gamma\alpha_{iv}}{A' + \gamma}, \qquad S_{iii} = \frac{S_e - \gamma\alpha_{ii}}{A' - \gamma}. \tag{C.2}$$

To solve Eq. (C.1), we make a substitution $w = S - \alpha$, which gives a separable differential equation in each interval (i) to (ii), and (iii) to (iv):

$$\left(\frac{1 + \frac{\kappa\gamma C}{S_e}w}{1 - \frac{CA'}{S_e}w}\right)\frac{\mathrm{d}w}{\mathrm{d}S} = 1. \tag{C.3}$$

We seek to calculate $\alpha_{ii}(S_{ii}, S_{iv})$ and $\alpha_{iv}(S_{ii}, S_{iv})$, which in turn yield the incremental damage per cycle according to Eq. (20).

Appendix C.1. Case $A' = 0$

For simple shear stress, when $\text{tr}(\boldsymbol{e}) = 0$, we have $A' = 0$, $\gamma = \sqrt{3/2}$, and Eq. (C.2) gives

$$S_i = \alpha_{iv} + \sqrt{\frac{2}{3}}S_e, \quad S_{iii} = \alpha_{ii} - \sqrt{\frac{2}{3}}S_e. \tag{C.4}$$

Moreover, Eq. (C.3) simplifies to

$$\left(1 + \sqrt{\frac{3}{2}}\frac{\kappa C}{S_e}w\right)\frac{\mathrm{d}w}{\mathrm{d}S} = 1. \tag{C.5}$$

Integration of Eq. (C.5) from (i) to (ii) with $\kappa = 1$, and from (iii) to (iv) with $\kappa = -1$, respectively, gives a system of Eqs.

$$-\frac{CS_e}{\sqrt{6}} + \frac{\sqrt{6}C}{4S_e}(S_{ii} - \alpha_{ii})^2 - \alpha_{ii} + \alpha_{iv} = 0, \tag{C.6a}$$

$$\frac{CS_e}{\sqrt{6}} - \frac{\sqrt{6}C}{4S_e}(\alpha_{iv} - S_{iv})^2 + \alpha_{ii} - \alpha_{iv} = 0. \tag{C.6b}$$

By adding Eq. (C.6b) to Eq. (C.6a) and using that $S_{ii} > \alpha_{ii} > \alpha_{iv} > S_{iv}$, we have

$$\Delta s = S_{ii} - \alpha_{ii} = \alpha_{iv} - S_{iv}, \tag{C.7}$$

for some stress difference $\Delta s \geq 0$. We insert $\Delta s = S_{ii} - \alpha_{ii}$ and $\alpha_{ii} - \alpha_{iv} = S_{ii} - S_{iv} - 2\Delta s$ into Eq. (C.6a), giving a second-order polynomial equation with one positive solution

$$\Delta s(S_{ii}, S_{iv}) = \sqrt{\frac{8}{3}}\frac{S_e}{C}\left[\sqrt{1 + \sqrt{\frac{3}{8}}\frac{C}{S_e}(S_{ii} - S_{iv}) + \frac{1}{4}C^2} - 1\right]. \tag{C.8}$$

We then obtain $\alpha_{ii} = S_{ii} - \Delta s(S_{ii}, S_{iv})$ and $\alpha_{iv} = S_{iv} + \Delta s(S_{ii}, S_{iv})$.

Appendix C.2. Case $0 < A' < \gamma$

For $0 < A' < \gamma$, integration of Eq. (C.3) from state (i) to (ii) with $\kappa = 1$, and from state (iii) to (iv) with $\kappa = -1$, respectively, gives a system of equations

$$\frac{S_e + \gamma\alpha_{ii}}{A' + \gamma} - S_{ii} - \frac{S_e}{A'C}\ln\frac{1 + \frac{A'C}{S_e}(\alpha_{ii} - S_{ii})}{1 + \frac{A'C}{S_e(A'+\gamma)}(A'\alpha_{iv} - S_e)} = 0, \tag{C.9a}$$

$$\frac{S_e - \gamma\alpha_{iv}}{A' - \gamma} - S_{iv} - \frac{S_e}{A'C}\ln\frac{1 + \frac{A'C}{S_e}(\alpha_{iv} - S_{iv})}{1 + \frac{A'C}{S_e(A'-\gamma)}(A'\alpha_{ii} - S_e)} = 0. \tag{C.9b}$$

With degenerate cases like $A' = \gamma$ excluded, this system of equations implicitly defines $\alpha_{ii}(S_{ii}, S_{iv})$ and $\alpha_{iv}(S_{ii}, S_{iv})$ such that $S_{ii} > \alpha_{ii} > \alpha_{iv} > S_{iv}$.

References

[1] Y. S. Garud, A new approach to the evaluation of fatigue under multiaxial loadings, J. Eng. Mater.-T. ASME 103 (2) (1981) 118–125. doi:10.1115/1.3224982.

[2] F. Morel, A critical plane approach for life prediction of high cycle fatigue under multiaxial variable amplitude loading, Int. J. Fatigue 22 (2) (2000) 101–119. doi:10.1016/S0142-1123(99)00118-8.
[3] N. S. Ottosen, R. Stenström, M. Ristinmaa, Continuum approach to high-cycle fatigue modeling, Int. J. Fatigue 30 (6) (2008) 996–1006. doi:10.1016/j.ijfatigue.2007.08.009.
[4] M. A. Meggiolaro, J. T. P. Castro, H. Wu, Non-linear incremental fatigue damage calculation for multiaxial non-proportional histories, Int. J. Fatigue 100 (2017) 502–511. doi:10.1016/j.ijfatigue.2016.12.008.
[5] S. Suresh, Fatigue of materials, Cambridge Solid State Science Series, Cambridge University Press, 1991.
[6] J. A. Bannantine, D. F. Socie, A variable amplitude multiaxial fatigue life prediction method, in: K. F. Kussmaul, D. L. McDiarmid, D. F. Socie (Eds.), Fatigue under biaxial and multiaxial loading, Vol. 10 of Mechanical engineering publications, European Structural Integrity Society, 1991, pp. 367–370.
[7] C. H. Wang, M. W. Brown, Life prediction techniques for variable amplitude multiaxial fatigue—Part 1: Theories, J. Eng. Meter. Technol. 118 (1996) 367–370.
[8] C. H. Wang, M. W. Brown, Life prediction techniques for variable amplitude multiaxial fatigue—Part 2: Comparison with experimental results, J. Eng. Meter. Technol. 118 (1996) 371–374.
[9] A. Franchi, F. Genna, P. Riva, Incremental elastic-Ziegler kinematic hardening plasticity formulations and an algorithm for the numerical integration with an "a priori" error control, in: D. E. Grierson, A. Franchi, P. Riva (Eds.), Progress in Structural Engineering, Springer Netherlands, Dordrecht, 1991, pp. 407–421.
[10] N. S. Ottosen, M. Ristinmaa, R. Kouhia, Enhanced multiaxial fatigue criterion that considers stress gradient effects, Int. J. Fatigue 116 (2018) 128–139.
[11] S. Holopainen, R. Kouhia, T. Saksala, Continuum approach for modelling transversely isotropic high-cycle fatigue, Eur. J. Mech. A 60 (2016) 183–195. doi:10.1016/j.euromechsol.2016.06.007.
[12] S. Holopainen, R. Kouhia, J. Könnö, T. Saksala, Computational modelling of transversely isotropic high-cycle fatigue using a continuum based model, Procedia Structural Integrity 2 (2016) 2718–2725, 21st European Conference on Fracture, ECF21, 20-24 June 2016, Catania, Italy. doi:10.1016/j.prostr.2016.06.339.
[13] T. Saksala, S. Holopainen, R. Kouhia, On the choice of damage variable in the continuum fatigue model based on a moving endurance surface, in: Proc. of XII Finnish Mechanics days, 2015, pp. 57–62.
[14] T. Frondelius, S. Holopainen, R. Kouhia, N. S. Ottosen, M. Ristinmaa, J. Vaara, A continuum based macroscopic unified low- and high-cycle fatigue model, MATEC Web of Conferences 300 (2019) 16008. doi:10.1051/matecconf/201930016008.
[15] R. Brighenti, A. Carpinteri, S. Vantadori, Fatigue life assessment under a complex multiaxial load history: an approach based on damage mechanics, Fatigue Fract. Eng. M. 35 (2) (2012) 141–153. doi:10.1111/j.1460-2695.2011.01600.x.
[16] P. Wynn, On a device for computing the $e_m(s_n)$ transformation, Math. Tables Aids Comput. 10 (54) (1956) 91–96.
[17] S. Suresh, S. B. Lindström, C.-J. Thore, B. Torstenfelt, A. Klarbring, Topology optimization using a continuous-time high-cycle fatigue model, Struct. Multidiscip. O. (2019).
[18] J. W. Eaton, D. Bateman, S. Hauberg, R. Wehbring, GNU Octave: A high-level interactive language for numerical computations, 4th Edition, 2018.
URL `https://octave.org/doc/interpreter/`
[19] R. C. Rice, J. L. Jackson, J. Bakuckas, S. Thompson, Metallic materials properties development and standardization, Tech. Rep. DOT/FAA/AR-MMPDS-01, U.S. Depertment of Transportation, Office of Aviation Research, Washington D.C. 20591 (January 2003).
[20] M. Mitchell, B. Muftakhidinov, T. W. *et al.*, Engauge Digitizer Software, http://markummitchell.github.io/engauge-digitizer (2019). doi:10.5281/zenodo.3370364.
[21] T. Zhao, Y. Jiang, Fatigue of 7075-T651 aluminum alloy, Int. J. Fatigue 30 (5) (2008) 834–849. doi:10.1016/j.ijfatigue.2007.07.005.
[22] I. V. Papadopoulos, Critical plane approaches in high-cycle fatigue: On the definition of the amplitude and mean value of the shear stress acting on the critical plane, Fatigue Fract. Engng Mater. Struct. 21 (1998) 269–285.
[23] L. Reis, B. Lin, M. de Freitas, Fatigue behaviour of a structural steel under non-proportional multiaxial loading, Ciência e Tecnologia dos Materiais 20 (2008) 87–91.
[24] V. Anes, L. Reis, B. Lin, M. de Freitas, New approach to evaluate non-proportionality in multiaxial loading conditions, Fatigue Fract. Eng. M. 37 (2014) 1338–1354. doi:10.1111/ffe.12192.
[25] B.-R. You, S.-B. Lee, A critical review on multiaxial fatigue assessments of metals, Int. J. Fatigue 18 (4) (1996) 235–244.
[26] H. Svärd, A branch and bound algorithm for evaluation of the Findley fatigue criterion, Int. J. Fatigue 73 (2015) 27–38. doi:10.1016/j.ijfatigue.2014.11.008.
[27] B. Weber, B. Kenmeugne, J. C. Clement, J. L. Robert, Improvements of multiaxial fatigue criteria computation for a strong reduction of calculation duration, Comp. Mater. Sci. 15 (4) (1999) 381–399. doi:10.1016/S0927-0256(98)00129-3.
[28] A. F. Filippov, Differential Equations with Discontinuos Righthand Sides, Kluwer Academic Publishers, Dordrecht, 1988.